Geometric uncertainty propagation in laminar flows solved by RBF-FD meshless technique

Geometric uncertainty propagation in laminar flows solved by RBF-FD meshless technique

R. Zamolo and L. Parussini

Dipartimento di Ingegneria e Architettura, Università degli Studi di Trieste, via A. Valerio 10, 34127 Trieste, Italy

E-mail: riccardo.zamolo@phd.units.it

Abstract. The Non-Intrusive Polynomial Chaos method is employed to analyze incompressible and laminar fluid flows in presence of geometric uncertainties on the boundaries, which are described by stochastic variables with known probability distribution. Non-Intrusive methods allow the use of existing deterministic solvers, which are treated as black boxes. Therefore the quantification of the fluid flow uncertainties is based on a set of deterministic response evaluations. The required thermo-fluid dynamics solutions over the deterministic geometries are obtained through a Radial Basis Function-generated Finite Differences (RBF-FD) meshless method. The validation of the presented approach is carried out through analytical test cases (isothermal flow between non-parallel walls) with one geometric uncertainty. The applicability of the presented approach to practical problems is then presented through the prediction of geometric uncertainty effects on the non-isothermal flow over a heated backward-facing step.

1. Introduction

Manufacturing tolerances in production processes lead to an uncertain behavior in the performance of the products, which must be taken into account when dealing with robust design. Therefore, it is important to develop efficient numerical approaches allowing the accurate quantification of such uncertainties. In this work we focus on the propagation of geometric uncertainties on the boundaries in incompressible, laminar and steady-state fluid flows.

The stochastic problems are solved by the Non-Intrusive Polynomial Chaos method [1–3]. This formulation allows the use of existing solvers as black boxes and the calculation of the random response is based on a set of deterministic response evaluations. The required numerical solutions over the deterministic geometries are obtained through a Radial Basis Function-generated Finite Differences (RBF-FD) meshless method [4–8]. This choice is due to the geometric flexibility and the ability of RBF-FD meshless methods to easily deal with general and complex-shaped domains, since a simple distribution of nodes over the domain is required only, and no mesh/grid/tessellation is needed. Furthermore, the order of accuracy of RBF-FD methods can be easily increased by using larger stencils, i.e., more nodes in the local RBF expansion [9].

The proposed approach is validated through different benchmark test cases and is then employed for the quantification of the statistical moments (expected value μ and variance σ^2) of the flow fields (velocity, pressure and temperature) in the case of a heated backward-facing step at $Re = 700$ where the position of the step corner is described by two stochastic variables with Gaussian distribution.

This paper is organized as follows: In the next section we introduce the governing equations of the an incompressible fluid flow, and in Section 3 we review the theory of the Tensorial-expanded Polynomial Chaos. In Section 4 we present the original meshless solver used to compute the deterministic flow field solutions needed by the adopted methodology for uncertainty quantification. In Section 5 we present the results obtained by the proposed approach.

2. Governing equations

Let us consider an incompressible fluid with density ρ, kinematic viscosity ν, thermal diffusivity α and thermal conductivity k. The resulting conservation equations of mass, momentum and energy are

$$\nabla \cdot \mathbf{u} = 0 \tag{1}$$

$$\frac{\partial \mathbf{u}}{\partial t} + (\mathbf{u} \cdot \nabla)\mathbf{u} = -\nabla p + \frac{1}{Re}\nabla^2 \mathbf{u} + \mathbf{F} \tag{2}$$

$$\frac{\partial T}{\partial t} + \mathbf{u} \cdot \nabla T = \frac{1}{RePr}\nabla^2 T. \tag{3}$$

In the above equations, length, velocity $\mathbf{u} = (u, v)$, time t, pressure p and temperature T, with a reference heat flux q, are made nondimensional by taking H, U_0, H/U_0, ρU_0^2 and qH/k as reference quantities, respectively. $Re = U_0 H/\nu$ is the flow Reynolds number, $Pr = \nu/\alpha$ is the Prandtl number and $\mathbf{F}$ is a nondimensional force per unit nondimensional volume. Buoyancy effects are neglected.

3. Uncertainty quantification

3.1. Tensorial-expanded Polynomial Chaos

Given a vector of M independent random variables $\boldsymbol{\xi} = (\xi_1, \ldots, \xi_M)^T$, under certain conditions [3] a random process $\phi(\boldsymbol{\xi})$, with finite second-order moments, which describes most physical processes, can be expanded as

$$\phi(\boldsymbol{\xi}) = \sum_{i=0}^{\infty} \phi_i \Psi_i(\boldsymbol{\xi}) \tag{4}$$

where $\{\Psi_i\}$ is a suitable basis and ϕ_i are the corresponding expansion coefficients. For each type of random variables distribution there exists the best representation, i.e., the best choice for the basis $\{\Psi_i\}$, in terms of convergence rate for the sought statistical moments of ϕ. In this work random variables with gaussian distribution $\xi_i \sim \mathcal{N}(0, 1)$ will be considered only, therefore the corresponding best representation is given by Hermite polynomials (Hermite-Chaos). In fact, 1D Hermite polynomials are orthogonal with respect to the gaussian probability density function (PDF), therefore the M-dimensional tensorial-expanded Hermite polynomials are orthogonal with respect to the M-dimensional gaussian PDF $w(\boldsymbol{\xi})$, given by

$$w(\boldsymbol{\xi}) = \prod_{k=1}^{M} \frac{e^{-\xi_k^2/2}}{\sqrt{2\pi}} = \frac{e^{-\boldsymbol{\xi}^T\boldsymbol{\xi}/2}}{(\sqrt{2\pi})^M}. \tag{5}$$

The expansion (4), expressed in the Hermite-Chaos form and truncated to a finite number $Q + 1$ of terms, is therefore

$$\phi(\boldsymbol{\xi}) \approx \sum_{i=0}^{Q} \phi_i \Psi_i(\boldsymbol{\xi}) = \sum_{i_1=0}^{q_1} \cdots \sum_{i_M=0}^{q_M} \phi_{i_1 \ldots i_M} H_{i_1}(\xi_1) \cdots H_{i_M}(\xi_M) \tag{6}$$

where $H_j(\xi) = (-1)^j e^{\xi^2/2} \frac{d^j}{d\xi^j} e^{-\xi^2/2}$ is the Hermite polynomial of degree j.

The statistical moments of ϕ can be computed from the approximation (6): the expected value $\mu(\phi)$ and the variance $\sigma^2(\phi)$ are

$$\mu(\phi) \approx \int_{\mathcal{R}^M} \phi(\boldsymbol{\xi}) w(\boldsymbol{\xi}) \mathrm{d}\boldsymbol{\xi} = \phi_{0\ldots0} \tag{7}$$

$$\sigma^2(\phi) \approx \int_{\mathcal{R}^M} \big(\phi(\boldsymbol{\xi}) - \phi_{0\ldots0}\big)^2 w(\boldsymbol{\xi}) \mathrm{d}\boldsymbol{\xi} = -\phi_{0\ldots0}^2 + \sum_{i_1=0}^{q_1} \cdots \sum_{i_M=0}^{q_M} \phi_{i_1\ldots i_M}^2 i_1! \cdots i_M!. \tag{8}$$

3.2. Collocation
In order to obtain the best approximation for $\mu(\phi)$ and $\sigma^2(\phi)$, we note that Eqs. (7)-(8) are weighted integrals with a gaussian weight function $w(\boldsymbol{\xi})$. Therefore, the best choice for the $Q+1 = (q_1+1)\cdots(q_M+1)$ sample points $\boldsymbol{\xi}^{(i)}$, i.e., the points where $\phi(\boldsymbol{\xi})$ has to be evaluated, are the roots of the Hermite polynomial of degree q_k+1 along each of the M dimensions

$$H_{q_k+1}\big(\xi_k^{(i)}\big) = 0 \qquad \text{for } k = 1, \ldots, M \text{ and } i = 1, \ldots, q_k+1. \tag{9}$$

The Hermite-Chaos expansion (6) is therefore made valid at each of the $Q+1$ sample points defined by Eq. (9), i.e, by using a collocation technique, in order to obtain the $Q+1$ unknown coefficients $\phi_{i_1\ldots i_M}$. In other words, the Hermite-Chaos expansion can be seen as an interpolant matching the random process ϕ at the sample points $\boldsymbol{\xi}^{(i)}$.

4. RBF-FD meshless method
The evaluation of the random process ϕ at the sample points $\boldsymbol{\xi}^{(i)}$ can be done with a suitable deterministic solver. Many both commercial and open-source solvers exist for solving Eqs. (1)-(2)-(3), but most of them need a mesh/grid/tessellation of the computational domain. If we analyze the effect of geometric uncertainties on the boundaries in the flow field, it means we have to solve the fluid dynamic problem on different computational domains. It easy to understand that a solver which does not need a mesh/grid/tessellation of the computational domain is a major advantage for the uncertainty quantification. In this perspective the RBF-FD meshless method is proposed.

4.1. RBF-FD discretization
4.1.1. 2D node distributions The 2D node distributions required by the RBF-FD meshless discretization have been obtained through the quadtree algorithm modified with a dithering correction and followed by repel refinement [9, 10]. The resulting distribution is a set of N nodes $\mathbf{x}_i$ which are isotropically displaced over the domain Ω and over its boundary $\Gamma = \partial\Omega$ according to a prescribed spacing function $s(\mathbf{x})$.

4.1.2. RBF interpolation A generic field ϕ is approximated near $\mathbf{x}$ by the following local RBF expansion

$$\phi(\mathbf{x}) = \sum_{i=1}^{n} a_i \varphi(\|\mathbf{x} - \mathbf{x}_{i'}\|) + \sum_{j=1}^{m} c_j g_j(\mathbf{x} - \bar{\mathbf{x}}) \tag{10}$$

where $i' = i'(\mathbf{x})$ are the indices of the $n = 25$ supporting nodes $\mathbf{x}_{i'}$ closest to $\mathbf{x}$, $\bar{\mathbf{x}}$ is their mean position, $\varphi(\|\cdot\|)$ are Radial Basis Functions (RBF) and a_i are the corresponding coefficients. The functions g_j form a complete 2D polynomial basis of degree $P = 3$ with $m = \binom{P+2}{P}$ terms and c_j are the corresponding coefficients. The choice of such a large stencil $n = 25$, compared to standard finite difference stencils, e.g., 5-point stencil, is due to two facts: the chosen polynomial

degree $P = 3$ requires $n \geq m = 10$ nodes while $n \geq 2m = 20$ is recommended in order to obtain more stable RBF-FD schemes which are less sensitive to the node arrangements [11–13]. The multiquadric RBF $\varphi(r) = \sqrt{1 + (\varepsilon r)^2}$ has been chosen [14], where the shape factor is chosen to be $\varepsilon = 0.4/s(\bar{\mathbf{x}})$ (see [9] for further details).

The expansion (10) is employed to match the unknown field ϕ at the $n_I \leq n$ supporting nodes $\mathbf{x}_k$ which do not lie on the boundary Γ

$$\phi(\mathbf{x}_k) = \sum_{i=1}^{n} a_i \varphi(\|\mathbf{x}_k - \mathbf{x}_{i'}\|) + \sum_{j=1}^{m} c_j g_j(\mathbf{x}_k - \bar{\mathbf{x}}) = \phi_k. \tag{11}$$

If any of the supporting nodes lie on the boundary Γ, i.e., $n_B = n - n_I$ boundary nodes $\mathbf{x}_b$, the expansion (10) is enforced to satisfy the corresponding boundary condition (BC)

$$\alpha\phi + \beta\frac{\partial\phi}{\partial\mathbf{n}} = \gamma \qquad \text{at } \mathbf{x} = \mathbf{x}_b \tag{12}$$

where α, β, γ are the coefficients for the Robin BC and $\mathbf{n}$ is the exterior normal to Γ.

In order to guarantee the polynomial reproduction, i.e., the exactness of expansion (10) for polynomials up to degree P, the following conditions are required

$$\sum_{i=1}^{n} a_i g_j(\mathbf{x}_{i'} - \bar{\mathbf{x}}) = 0 \qquad j = 1, \ldots, m. \tag{13}$$

By collecting the $n_I + n_B + m = n + m$ conditions expressed by Eqs. (11)-(12)-(13), the following local linear system is obtained

$$\mathbf{B}\begin{pmatrix}\mathbf{a}\\ \mathbf{c}\end{pmatrix} = \begin{pmatrix}\boldsymbol{\phi}\\ \boldsymbol{\gamma}\\ \mathbf{0}\end{pmatrix} \tag{14}$$

where $\mathbf{B} \in \mathbb{R}^{(n+m)\times(n+m)}$ is nonsingular, $\mathbf{a} = (a_i) \in \mathbb{R}^n$, $\mathbf{c} = (c_j) \in \mathbb{R}^m$, $\boldsymbol{\phi} = (\phi_k) \in \mathbb{R}^{n_I}$, $\boldsymbol{\gamma} = \big(\gamma(\mathbf{x}_b)\big) \in \mathbb{R}^{n_B}$ and $\mathbf{0} \in \mathbb{R}^m$ are column vectors. The compact notation for the expansion (10) is

$$\phi(\mathbf{x}) = \begin{pmatrix}\boldsymbol{\varphi}\\ \mathbf{g}\end{pmatrix}^T\begin{pmatrix}\mathbf{a}\\ \mathbf{c}\end{pmatrix} \tag{15}$$

where $\boldsymbol{\varphi} = \Big(\varphi(\|\mathbf{x} - \mathbf{x}_{i'}\|)\Big) \in \mathbb{R}^n$ and $\mathbf{g} = \Big(g_j(\mathbf{x} - \bar{\mathbf{x}})\Big) \in \mathbb{R}^m$ are also column vectors.

4.1.3. RBF-FD collocation Given the following linear partial differential equation in the unknown field ϕ

$$\mathcal{L}(\phi) = f \tag{16}$$

where $\mathcal{L}$ is a linear operator and f is a known function, Eq. (16) is made valid at each node $\mathbf{x}_i$ which do not lie on the boundary Γ using the RBF expansion (15) and Eq. (14) for the expansion coefficients $\mathbf{a}$ and $\mathbf{b}$

$$\begin{pmatrix}\mathcal{L}(\boldsymbol{\varphi})\\ \mathcal{L}(\mathbf{g})\end{pmatrix}^T\begin{pmatrix}\mathbf{a}\\ \mathbf{c}\end{pmatrix} = \begin{pmatrix}\mathcal{L}(\boldsymbol{\varphi})\\ \mathcal{L}(\mathbf{g})\end{pmatrix}^T\mathbf{B}^{-1}\begin{pmatrix}\boldsymbol{\phi}\\ \boldsymbol{\gamma}\\ \mathbf{0}\end{pmatrix} = \mathbf{l}^T\begin{pmatrix}\boldsymbol{\phi}\\ \boldsymbol{\gamma}\\ \mathbf{0}\end{pmatrix} = f \qquad \text{at } \mathbf{x} = \mathbf{x}_i \tag{17}$$

where the operator $\mathcal{L}$ is applied to the RBF basis $\boldsymbol{\varphi}$ and to the polynomial basis $\mathbf{g}$ because of the linearity of $\mathcal{L}$. Eq. (17) is the final equation for node $\mathbf{x}_i$ and shows that the stencil coefficients, i.e., the first n_I components of vector $\mathbf{l}$, can be computed by solving the following linear system

$$\mathbf{B}^T\mathbf{l} = \begin{pmatrix}\mathcal{L}(\boldsymbol{\varphi})\\ \mathcal{L}(\mathbf{g})\end{pmatrix} \qquad \text{at } \mathbf{x} = \mathbf{x}_i. \tag{18}$$

4.2. Solution procedure

At each time step, the computation of velocity, pressure and temperature through Eqs. (1)-(2)-(3) is decoupled using a projection scheme with a three-level Gear scheme for the time discretization. A tentative velocity $\mathbf{u}^*$ is computed from the linearized momentum equation

$$\frac{3\mathbf{u}^* - 4\mathbf{u}^l + \mathbf{u}^{l-1}}{2\Delta t} + \mathbf{u}^l \nabla \mathbf{u}^* = -\nabla p^l + \frac{1}{Re}\nabla^2 \mathbf{u}^* + \mathbf{F} \tag{19}$$

where l is the time level and $\Delta t = 1.5$ is the chosen nondimensional time step size. $\mathbf{u}^*$ is then forced to satisfy the continuity equation (1) by means of an irrotational correction $\mathbf{u}^{l+1} = \mathbf{u}^* - \nabla\Phi$, leading to the following Poisson equation in the auxiliary variable Φ with homogeneous Neumann BC

$$\nabla^2 \Phi = \nabla \cdot \mathbf{u}^*. \tag{20}$$

The pressure is updated as $p^{l+1} = p^l + \Phi/\Delta t$ and the temperature is computed from

$$\frac{3T^{l+1} - 4T^l + T^{l-1}}{2\Delta t} + \mathbf{u}^{l+1}\nabla T^{l+1} = \frac{1}{RePr}\nabla^2 T^{l+1}. \tag{21}$$

Eqs. (19)-(20)-(21) are discretized with the same RBF-FD scheme presented in Section 4.1 employing an explicit stabilization with ∇^6 hyperviscosity [9] and $\delta_6 = 5 \times 10^{-5}$. A BiCGSTAB iterative solver [15] with an incomplete LU factorization [16] as preconditioner are employed for the solution of the transport Eqs. (19) and (21) using a relative tolerance $tol = 10^{-10}$, while the Poisson Eq. (20) is solved through a LU decomposition which can be performed once at the beginning of the simulation. The steady-state convergence is declared when

$$\frac{\|\mathbf{u}^{l+1} - \mathbf{u}^l\|_2}{Re\Delta t\sqrt{2N}} < 10^{-9}. \tag{22}$$

5. Results

5.1. Validation of the RBF-FD method

A steady flow over a backward-facing step at $Re = 800$ is considered as benchmark test case. The geometry of the problem is depicted in Figure 1, together with the employed spacing function s and a particular of a node distribution with $N = 50,000$ nodes. Higher node density, i.e., number of nodes per unit area, is employed near the walls in order to accurately solve the wall gradients. The domain extends till $x/H = 30$, where h is the channel height upstream of the step and $H = 2h$ is the downstream channel height. A parabolic velocity profile $u = 6U_0\frac{y}{h}(1-\frac{y}{h})$ is imposed at the inlet ($x/h = -3$) while fully developed flow conditions $\frac{\partial \mathbf{u}}{\partial x} = 0$ with $p = 0$ are imposed at the outlet ($x/H = 30$).

A comparison between the computed velocity profiles for $N = 50,000$ and $N = 100,000$ nodes and the profiles calculated by Erturk [17] is depicted in Figure 2 for $x/h = 6$ and $x/h = 14$. A comparison between the normalized locations of detachment and reattachment of the flow (see [17] for the definitions) is reported in Table 1, where the results obtained with a commercial finite volume solver (ANSYS Fluent) are also shown as reference. Cartesian grids have been employed in the latter case, where the cell dimensions follow approximately the spacing function s near the walls, while a steady-state formulation and a third-order upwind scheme have been employed. Both the previous comparisons show a very good agreement with the reference results, therefore $N = 50,000$ nodes are employed for the following calculations. Furthermore, the computed streamlines depicted in Figure 3 agree very well, to graphical accuracy, with the ones reported in [17]. Despite the actual problem that will be faced in Subsection 5.3 is not isothermal, the properties of the RBF-FD discretization of energy Eq. (3) are comparable to the ones of momentum Eq. (2) since they are formally equivalent ($Pr = 0.71 \approx 1$) and the

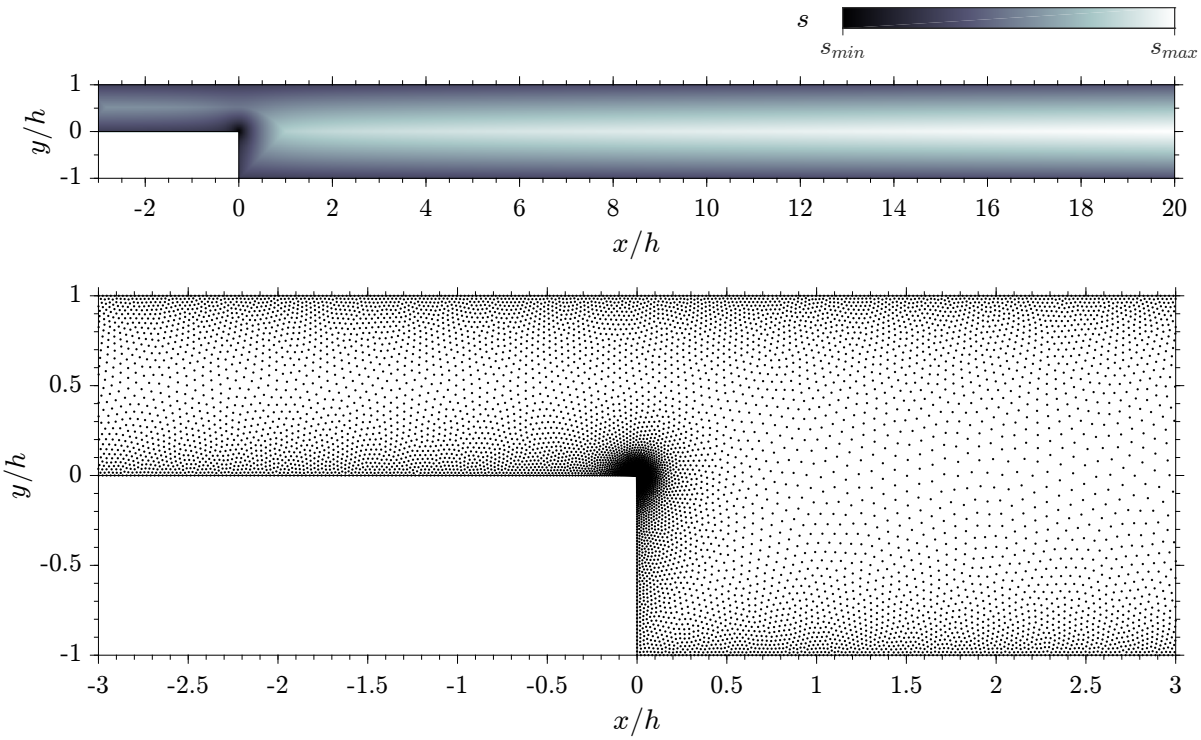

Figure 1. Backward-facing step: geometry and spacing function s (top), particular of the node distribution with $N = 50,000$ nodes (bottom).

discretization scheme is the same, therefore the present validation of the isothermal model can be extended to the non-isothermal model employed in Subsection 5.3. Furthermore, buoyancy effects are neglected in the momentum Eq. (2) and therefore the temperature does not affect the flow, i.e, no two-way coupling.

The computational times needed to reach the steady-state, i.e., Eq. (22), for the RBF-FD method with $N = 50,000$ and $N = 100,000$ nodes is approximately 3 and 6 minutes, respectively, on a modern laptop equipped with an Intel® i7 2.6GHz processor with 4 cores and a MATLAB implementation which automatically exploits the multi-core parallelism for the employed solvers. The computational times required by the Fluent simulation to reach a comparable level of convergence with $50,000$ and $100,000$ cells is approximately 50 seconds and

Table 1. Normalized locations of detachment and reattachment of the flow over the backward-facing step at $Re = 800$ (see [17] for the definitions).

	X0	Y0	X1	X2	X3
Erturk [17]	0.154	0.138	11.834	9.476	20.553
Fluent, 50k cells	0.123	0.113	11.665	9.464	20.341
Fluent, 100k cells	0.139	0.132	11.726	9.468	20.397
RBF-FD, 50k nodes	0.148	0.138	11.765	9.482	20.425
RBF-FD, 100k nodes	0.154	0.152	11.782	9.442	20.482

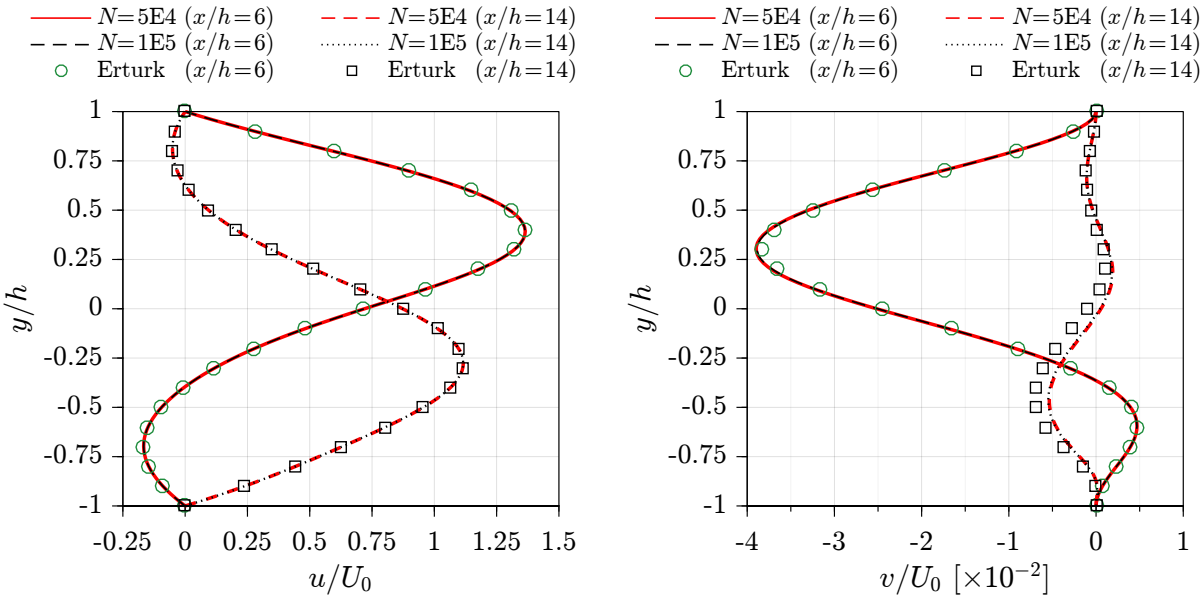

Figure 2. Flow over a backward-facing step at $Re = 800$: comparison of horizontal velocity u (left) and vertical velocity v (right).

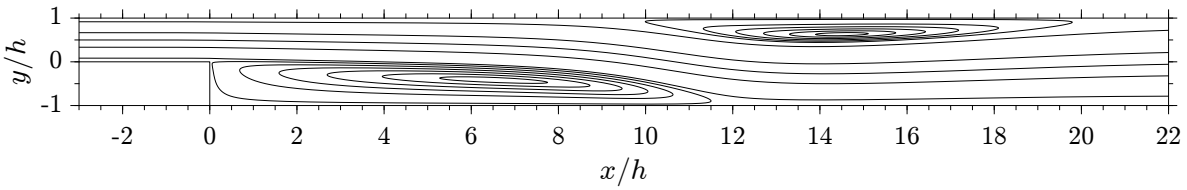

Figure 3. Flow over a backward-facing step at $Re = 800$: streamlines.

1.5 minutes, respectively, on the same machine by using 8 processes (2 threads per core) in order to fully exploit the multi-core parallelism. Note that the employed RBF-FD scheme has third order accuracy [9], while the Fluent finite volume scheme has second order accuracy.

5.2. Validation of the Hermite-Chaos method

The Stokes flow between two non-parallel walls, whose analytical solution is reported in Appendix A, is considered as benchmark test case with $L/H = 20$. A single geometric uncertainty is considered on the geometrical deviation $\delta = \xi_1 H/100$. The expected value μ and the standard deviation σ of velocities u and v and the pressure p are computed in the flow field.

In the first case the Hermite-Chaos method is employed on the analytical solution reported in Appendix A. The normalized RMS errors (NRMSE) for the expected value μ and for the standard deviation σ are shown in Figure 4 as functions of the degree q_1 of the Hermite-Chaos expansion (6).

In the second case the Hermite-Chaos method is employed on the numerical solutions provided by the RBF-FD method with $N = 50,000$ nodes and a constant spacing function. The corresponding normalized RMS errors for μ and for σ are shown in Figure 5.

A comparison between Figure 4 and Figure 5 reveals that for $q_1 \geq 3$ the error in the statistical moments is governed by the numerical error of the RBF-FD method, therefore a degree $q_k = 3$

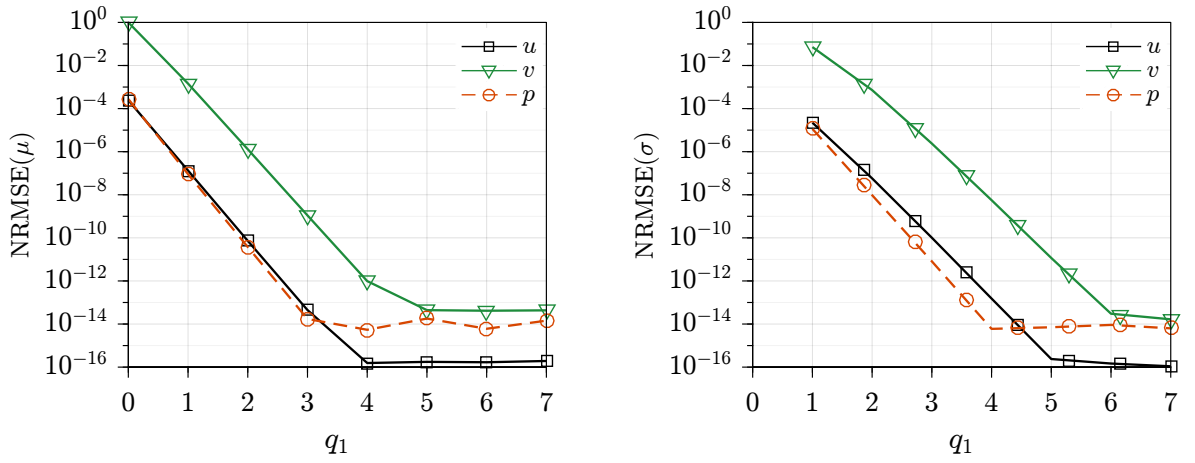

Figure 4. Stochastic stokes flow between non-parallel walls, analytical solution: normalized RMS error for the expected value μ (left) and for the standard deviation σ (right).

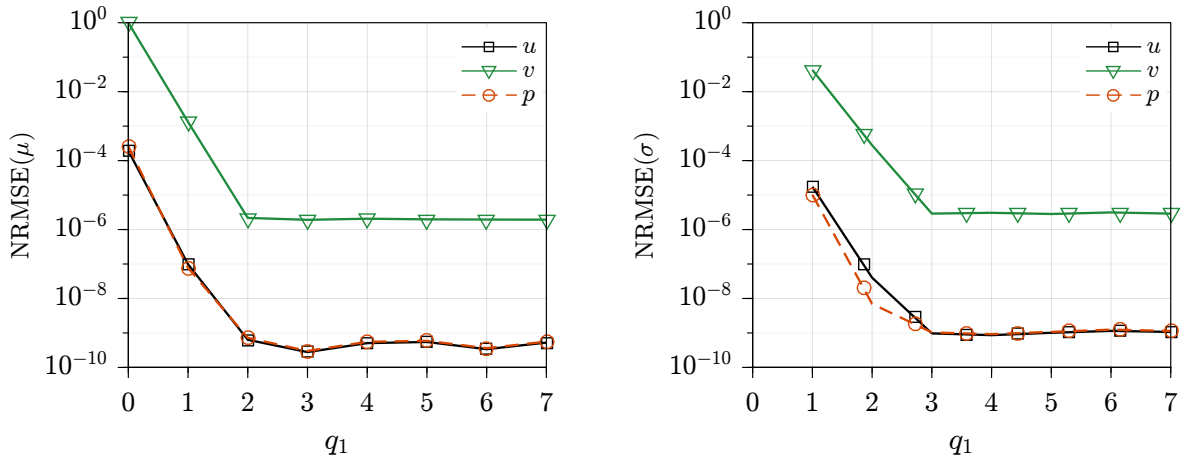

Figure 5. Stochastic stokes flow between non-parallel walls, numerical solution (RBF-FD): normalized RMS error for the expected value μ (left) and for the standard deviation σ (right).

for the Hermite-Chaos expansion is employed for the following calculations.

5.3. Uncertainty quantification in a heated backward-facing step

A heated backward-facing step at $Re = 700$ with $Pr = 0.71$ is considered, where a heat flux q is imposed at the bottom wall at $y/h = -1$, the temperature at the inlet is $T = 0$, a fully developed flow condition $\frac{\partial T}{\partial x} = 0$ is imposed at the outlet and the remaining walls are adiabatic. The BC for the velocities and pressure are the same of the case reported in Section 5.1, as well as the spacing function s. $N = 50,000$ nodes are employed. The position of the step corner $\mathbf{x}_C = (x_C, y_C) = \frac{H}{100}(\xi_1, \xi_2)$ is defined by $M = 2$ uncertain variables with normal distribution and polynomial degrees $q_1 = q_2 = 3$ are employed for the Hermite-Chaos expansion, requiring $Q + 1 = (q_1 + 1)(q_2 + 1) = 16$ deterministic RBF-FD solutions over the corresponding step geometries, where the step walls remain straight but not aligned to the x and y axes.

The expected value and the standard deviation of u, v, p, and T are depicted in Figures 6-9, where the streamlines are also shown. As expected, the standard deviation for u and v is higher in correspondence of the step corner and also where the flow exhibits large gradients and large

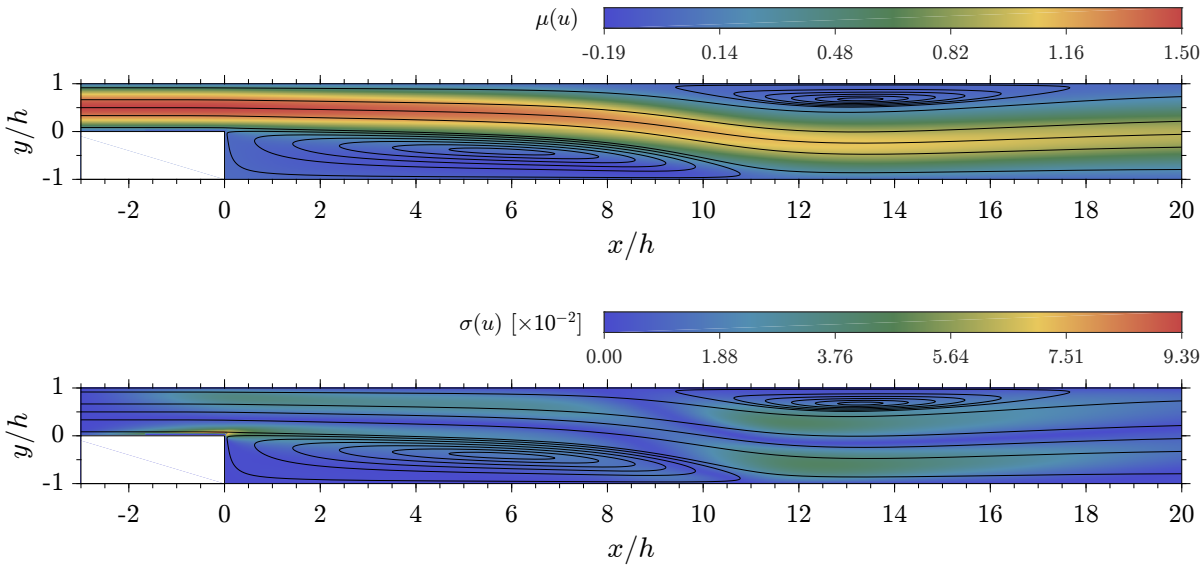

Figure 6. Stochastic flow over a heated backward-facing step at $Re = 700$: expected value μ (top) and standard deviation σ (bottom) for the horizontal velocity u.

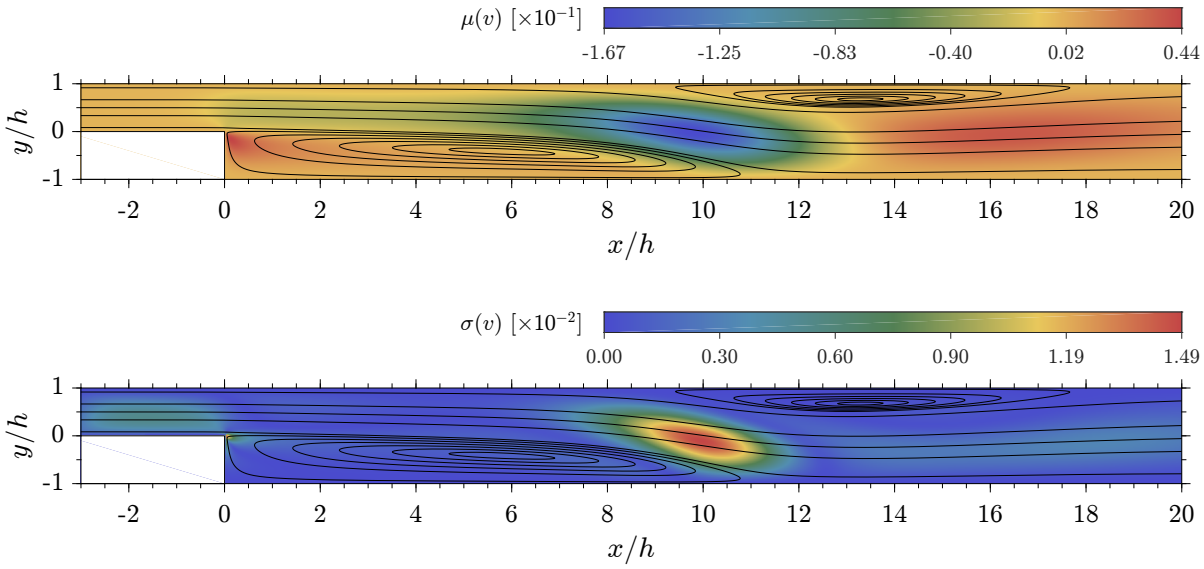

Figure 7. Stochastic flow over a heated backward-facing step at $Re = 700$: expected value μ (top) and standard deviation σ (bottom) for the vertical velocity v.

magnitudes in the velocities at the same time. For example, for u this occurs halfway between the streamline starting at the inlet at $y/h = 1/2$ (median streamline) and the streamlines starting at the inlet at $y/h = \{0, 1\}$ excluding the recirculation bubbles, while for v this occurs when the median streamline sustains the largest deviation from the horizontal direction, in between the detachment point of the upper recirculation bubble and the reattachment point of the lower one. The standard deviation of the pressure, Figure 8, is lower near the reattachment point of the lower recirculation bubble and higher at the lower zone of the inlet. The previous results are in perfect accordance with the ones obtained in [18] for $Re = 600$.

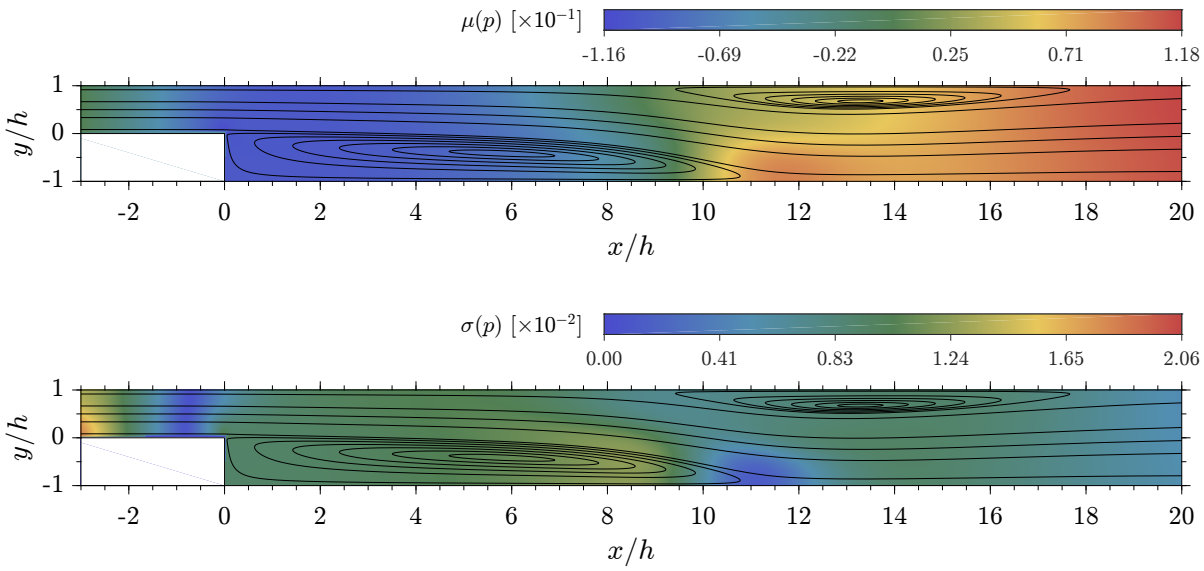

Figure 8. Stochastic flow over a heated backward-facing step at $Re = 700$: expected value μ (top) and standard deviation σ (bottom) for the pressure p.

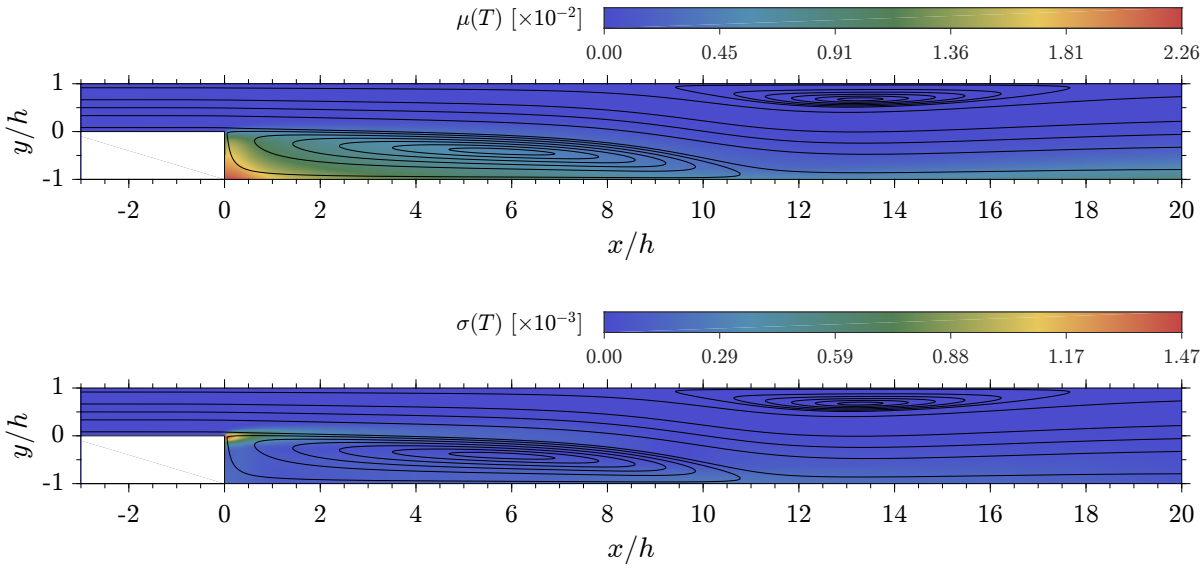

Figure 9. Stochastic flow over a heated backward-facing step at $Re = 700$: expected value μ (top) and standard deviation σ (bottom) for the temperature T.

As expected, the standard deviation of the temperature, Figure 9, is higher near the step corner and also in the downstream direction of the flow from the corner. This is quite obvious since in the lower recirculation bubble, which starts immediately below the corner, the temperature is high because of the recirculating flow subject to the heat flux q from below.

The computational time required for the quantification of the uncertainty in this case is approximately 30 minutes on the same machine described in Subsection 5.1. Note that in this particular case the total computational time is significantly less than 16 times the computational time of a single steady state computation since each of the $Q + 1 = 16$ deterministic solutions

is computed by starting from the steady solution obtained for the original geometry of the backward-facing step, i.e., $(\xi_1, \xi_2) = (0, 0)$, $\mathbf{x}_C = (0, 0)$.

6. Conclusions

In this work a Non-Intrusive Polynomial Chaos method is coupled to a RBF-FD meshless method for the accurate quantification of the uncertainties arising in laminar, incompressible and steady flows due to geometric uncertainties on the boundaries. The statistical moments of the flow fields, e.g., expected value and variance, are accurately calculated using the minimum number of deterministic fluid-flow solutions by means of the tensorial-expanded Hermite-Chaos formulation. Different test cases are successfully carried out in order to validate the procedure which is then employed to evaluate the propagation of the geometric uncertainties of the position of the step corner in a heated backward-facing step at $Re = 700$. Consistent results are found, suggesting that the presented approach can be used for the efficient quantification of the uncertainties in fluid flow problems on practical geometries.

The main advantage of the presented meshless approach over standard mesh-based approaches is its capability to easily deal with complex geometries, which turns out to be an additional advantage when coupling the RBF-FD method to the employed Non-Intrusive Polynomial Chaos method. This is due to the fact that the Non-Intrusive formulation requires multiple deterministic solutions over different geometries where meshless node distributions can be automatically, effectively and easily generated, while accuracy and computational costs are comparable to standard mesh-based methods. When dealing with practical problems with complex geometries, such an accuracy as that obtained in the test case of Subsection 5.2, i.e., NRMSE $\approx 10^{-6} - 10^{-9}$, is generally achievable with large number of nodes/cells and/or high order methods with relevant computational costs. From this perspective, the coupling of the RBF-FD meshless method to the Non-Intrusive Polynomial Chaos method is again favourable since arbitrary order RBF-FD schemes can be employed, while the Polynomial Chaos formulation requires the minimum number of deterministic solutions allowing a spectral convergence of the statistical moments.

Future work involving the presented methodology will deal with the prediction of geometric uncertainty effects for general heat transfer problems defined over 3D complex-shaped domains.

Appendix A. Stokes flow between non-parallel walls

Given an horizontal channel with length L between two non-parallel walls at $y = 0$ and $y = y_T(x) = H + x\delta/L$ $(x \in [0, L])$, an approximate solution to the Stokes equations, i.e, steady-state and isothermal Navier-Stokes Eqs. (1)-(2) where the convective term is neglected, is given in terms of streamfunction $\psi_T(x, y) = H\psi(y/y_T(x))$ where $\frac{\mathrm{d}\psi(\eta)}{\mathrm{d}\eta} = 6\eta(1 - \eta)$ is the parabolic profile and $\eta \in [0, 1]$. The pressure is

$$p = \frac{6}{y_T^2}\Big[\frac{L}{\delta} + \frac{\delta}{L}\Big(\frac{2y}{y_T} - \frac{3y^2}{y_T^2}\Big)\Big] \tag{A.1}$$

and the force in the momentum Eq. (2) is $\mathbf{F} = \big(\mathcal{O}(\delta^2), \mathcal{O}(\delta^3)\big)$.

References

[1] Hosder S, Walters R and Perez R 2006 A non-intrusive polynomial chaos method for uncertainty propagation in cfd simulations *44th AIAA Aerospace Sciences Meeting and Exhibit, Reno, Nevada*

[2] Eldred M 2009 Recent advances in non-intrusive polynomial chaos and stochastic collocation methods for uncertainty analysis and design *50th AIAA/ASME/ASCE/AHS/ASC Structures, Structural Dynamics, and Materials Conference, Palm Springs, California*

[3] Xiu D and Karniadakis G 2002 *SIAM J. Sci. Comput.* **24**(2) 619–644

[4] Li H and Mulay S 2013 *Meshless Methods and Their Numerical Properties* (CRC Press) ISBN 978-1-4665-1747-9
[5] Šarler B and Vertnik R 2006 *Comput. Math. Appl.* **51**(8) 1269–1282
[6] Waters J and Pepper D 2015 *Numer. Heat. Tr. B-Fund.* **68**(3) 185–203
[7] Fornberg B and Flyer N 2015 *Acta Numer.* **24** 215–258
[8] Zamolo R and Nobile E 2019 *Numer. Heat. Tr. B-Fund.* **75**(1) 19–42
[9] Zamolo R 2019 *Radial Basis Function-Finite Difference Meshless Methods for CFD Problems* Ph.D. thesis Universit degli Studi di Trieste Trieste, Italy
[10] Zamolo R and Nobile E 2018 *Comput. Math. Appl.* **75**(1) 4305–4321
[11] Flyer N, Fornberg B, Bayona V and Barnett G 2016 *J. Comput. Phys.* **321** 21–38
[12] Bayona V, Flyer N, Fornberg B and Barnett G 2017 *J. Comput. Phys.* **332** 257–273
[13] Bayona V, Flyer N and Fornberg B 2019 *J. Comput. Phys.* **380** 378–399
[14] Sarra S and Kansa E 2009 *Multiquadric Radial Basis Function Approximation Methods for the Numerical Solution of Partial Differential Equations* (*Advances in Computational Mechanics* vol 2) ed Atluri S (Tech Science Press)
[15] van der Vorst H 1992 *SIAM J. Sci. Stat. Comp.* **13**(2) 631–644
[16] Saad Y 2003 *Iterative Methods for Sparse Linear Systems* (Philadelphia, Pennsylvania: SIAM) chap 10: Preconditioning Techniques 2nd ed
[17] Erturk 2008 *Comput. Fluids* **37**(6) 633–655
[18] Parussini L, Pediroda V and Poloni C 2010 *Comput. Fluids* **39**(1) 137–151